GEOPHYSICS, VOL. 77, NO. 6 (NOVEMBER-DECEMBER 2012); P. U87–U96, 9 FIGS., 3 TABLES.
10.1190/GEO2012-0032.1

Migration velocity analysis for TI media in the presence of quadratic lateral velocity variation

Mamoru Takanashi[1] and Ilya Tsvankin[2]

ABSTRACT

One of the most serious problems in anisotropic velocity analysis is the trade-off between anisotropy and lateral heterogeneity, especially if velocity varies on a scale smaller than the maximum offset. We have developed a P-wave MVA (migration velocity analysis) algorithm for transversely isotropic (TI) models that include layers with small-scale lateral heterogeneity. Each layer is described by constant Thomsen parameters ε and δ and the symmetry-direction velocity V_0 that varies as a quadratic function of the distance along the layer boundaries. For tilted TI media (TTI), the symmetry axis is taken orthogonal to the reflectors. We analyzed the influence of lateral heterogeneity on image gathers obtained after prestack depth migration and found that quadratic lateral velocity variation in the overburden can significantly distort the moveout of the target reflection. Consequently, medium parameters beneath the heterogeneous layer(s) are estimated with substantial error, even when borehole information (e.g., check shots or sonic logs) is available. Because residual moveout in the image gathers is highly sensitive to lateral heterogeneity in the overburden, our algorithm simultaneously inverts for the interval parameters of all layers. Synthetic tests for models with a gently dipping overburden demonstrate that if the vertical profile of the symmetry-direction velocity V_0 is known at one location, the algorithm can reconstruct the other relevant parameters of TI models. The proposed approach helps increase the robustness of anisotropic velocity model-building and enhance image quality in the presence of small-scale lateral heterogeneity in the overburden.

INTRODUCTION

Anisotropic parameter estimation has become an essential part of a wide range of seismic imaging and reservoir-characterization projects (e.g., Tsvankin et al., 2010). Ignoring anisotropy can lead to mispositioning of horizontal and dipping reflectors, poor focusing of dipping events, etc. (Alkhalifah and Larner, 1994; Alkhalifah et al., 1996). Migration velocity analysis (MVA) has been extended to heterogeneous transversely isotropic media with a vertical (VTI) and tilted (TTI) symmetry axis (e.g., Sarkar and Tsvankin, 2004; Biondi, 2007; Behera and Tsvankin, 2009; Bakulin et al., 2010b, 2010c). Numerous field examples demonstrate that application of prestack depth migration (PSDM) with anisotropic MVA yields significantly improved images in the Gulf of Mexico and other regions (Calvert et al., 2008; Huang et al., 2008; Neal et al., 2009; Bakulin et al., 2010a).

However, anisotropic velocity analysis suffers from trade-offs between anisotropy parameters, lateral velocity variation, and the shapes of the reflecting interfaces. To make parameter estimation more stable, existing algorithms often keep the anisotropy parameters ε and/or δ fixed during iterative parameter updates (Charles et al., 2008; Huang et al., 2008).

Sarkar and Tsvankin (2003, 2004) present a 2D MVA algorithm designed to estimate the spatially varying velocity along with the parameters ε and δ of VTI media. They divide the model into factorized blocks, in which the ratios of the stiffness coefficients c_{ij} and, therefore, the anisotropy parameters are constant (Červený, 1989). The vertical velocity V_0 in each factorized block can vary in arbitrary fashion with the spatial coordinates (Červený, 1989), but Sarkar and Tsvankin (2003, 2004) employ the simplest, linear $V_0(x, z)$ function:

$$V_0(x, z) = V_0(0, 0) + k_{x1}x + k_{z1}z, \tag{1}$$

Manuscript received by the Editor 26 January 2012; revised manuscript received 15 July 2012; published online 8 October 2012.
[1]Colorado School of Mines, Department of Geophysics, Center for Wave Phenomena, Golden, Colorado, U.S.A.; and Japan Oil, Gas and Metals National Corporation, Chiba, Japan. E-mail: takanashi-mamoru@jogmec.go.jp.
[2]Colorado School of Mines, Department of Geophysics, Center for Wave Phenomena, Golden, Colorado, U.S.A. E-mail: ilya@dix.mines.edu.

where k_{x1} and k_{z1} are the horizontal and vertical velocity gradients, respectively. If V_0 is known at a single point in each factorized VTI block, the MVA algorithm can estimate the parameters ε and δ along with the velocity gradients. Two reflectors in each block, sufficiently separated in depth, are required for constraining the vertical gradient k_{z1}. It is also essential to use long-spread data (the spreadlength-to-depth ratio should reach at least two) or dipping events (the dip should exceed 25°–30°) to estimate ε (or the anellipticity parameter η). Application of this algorithm to a data set from West Africa produces a higher-quality image and more accurate velocity field compared with that generated by anisotropic *time* processing (Sarkar and Tsvankin, 2006). Behera and Tsvankin (2009) develop a similar MVA methodology for TTI media under the assumption that the symmetry axis is orthogonal to reflectors. Because the symmetry-axis orientation generally varies with reflector shape, TTI blocks are not "fully" factorized, even though ε and δ in each block are constant.

Most existing methods, however, are designed for relatively large-scale lateral heterogeneity. Lateral velocity variation on a scale comparable to or smaller than spreadlength (e.g., caused by velocity lenses) can distort the estimated parameters and reduce the quality of stack, even when the structure is relatively simple (Al-Chalabi, 1979; Toldi, 1989; Blias, 2009). In principle, both anisotropy and heterogeneity can be handled by grid-based reflection tomography (Woodward et al., 2008; Bakulin et al., 2010b, 2010c). However, small-scale lateral heterogeneity may produce significant errors in iterative tomographic inversion (Takanashi et al., 2009), especially because of pronounced nonuniqueness in anisotropic tomography (Bakulin et al., 2010b, 2010c).

Here, we extend the MVA algorithms of Sarkar and Tsvankin (2004) and Behera and Tsvankin (2009) to TI media with quadratic lateral variation of the symmetry-direction velocity V_0. The model is composed of "quasi-factorized" TI blocks with constant values of ε and δ and the symmetry axis orthogonal to the reflectors. First, we show that quadratic lateral velocity variation in a thin layer in the overburden produces residual moveout and causes distortions in parameter estimation for the target interval. To exploit the sensitivity of residual moveout to small-scale lateral heterogeneity in the overburden, we devise an MVA algorithm that simultaneously estimates the interval parameters in the target layers and overburden. Synthetic tests demonstrate that the presented method can accurately reconstruct the velocity field for TI models with thin laterally heterogeneous layers, if some a priori information about the symmetry-direction velocity is available.

INFLUENCE OF QUADRATIC LATERAL VELOCITY VARIATION ON IMAGE GATHERS

First, we analyze the influence of lateral velocity variation occurring on the scale of spreadlength for piecewise-factorized VTI models. By adding a quadratic term in the horizontal coordinate to equation 1, the vertical velocity V_0 in each block can be written as

$$V_0(x,z) = V_0(0,0) + k_{x1}x + k_{z1}z + k_{x2}x^2. \tag{2}$$

Note that the coefficient k_{x2} has different units ($s^{-1}\,m^{-1}$) than the velocity gradient k_{x1} (s^{-1}). A smooth (e.g., parabola-shaped) low-velocity lens centered near $x = 0$ can be approximated by the function $V_0(x,z)$ with a positive coefficient k_{x2}. Likewise, a high-velocity lens can be characterized by a negative k_{x2}.

Takanashi and Tsvankin (2012) discuss the influence of thin laterally heterogeneous (LH) layers on the reflection moveout from deeper interfaces. They show that the distortion of the NMO velocity or ellipse depends on the curvature (second spatial derivatives) of the vertical interval traveltime surface and increases with the distance between the LH layer and the target. Although Takanashi and Tsvankin (2012) present general 3D moveout equations for wide-azimuth data, here we use their results for 2D geometry (i.e., the acquisition line coincides with a vertical symmetry plane). It is also assumed that each layer has a horizontal symmetry plane (e.g., VTI) and both anisotropy and lateral heterogeneity are weak. In the special case of a medium composed of three horizontal layers with lateral heterogeneity confined to the second layer, the NMO velocity from the bottom of the model is given by (Takanashi and Tsvankin, 2012)

$$V_{\mathrm{NMO,het}}^{-2} = V_{\mathrm{NMO,hom}}^{-2} + \frac{\tau_0\, D}{3}\,\frac{\partial^2 \tau_{02}}{\partial x^2}, \tag{3}$$

$$D = k^2 + 3kl + 3l^2, \tag{4}$$

$$k = \frac{\tau_{02}\left(V_{\mathrm{NMO,hom}}^{(2)}\right)^2}{\tau_{01}\left(V_{\mathrm{NMO,hom}}^{(1)}\right)^2 + \tau_{02}\left(V_{\mathrm{NMO,hom}}^{(2)}\right)^2 + \tau_{03}\left(V_{\mathrm{NMO,hom}}^{(3)}\right)^2}, \tag{5}$$

and

$$l = \frac{\tau_{03}\left(V_{\mathrm{NMO,hom}}^{(3)}\right)^2}{\tau_{01}\left(V_{\mathrm{NMO,hom}}^{(1)}\right)^2 + \tau_{02}\left(V_{\mathrm{NMO,hom}}^{(2)}\right)^2 + \tau_{03}\left(V_{\mathrm{NMO,hom}}^{(3)}\right)^2}, \tag{6}$$

where $V_{\mathrm{NMO,het}}$ and τ_0 are the NMO velocity and zero-offset traveltime for the bottom of the model, $V_{\mathrm{NMO,hom}}$ is the NMO velocity for the reference laterally homogeneous (but vertically heterogeneous) medium with the parameters corresponding to the common-midpoint (CMP) location, and $V_{\mathrm{NMO,hom}}^{(m)}$ and τ_{0m} ($m = 1, 2, 3$) are the reference (background) interval NMO velocity and zero-offset interval traveltime in layer m. If the vertical variation of V_0 is mild, the parameters k and l are close to the thicknesses of the second and third layer, respectively, divided by the total thickness of the model.

The second derivative of the vertical traveltime can be replaced with that of the vertical velocity using the following approximate relationship (Grechka and Tsvankin, 1999):

$$\frac{\partial^2 \tau_{02}}{\partial x^2}\, V_{02} + \frac{\partial^2 V_{02}}{\partial x^2}\, \tau_{02} = 0, \tag{7}$$

where V_{02} is the vertical velocity in the second layer. If V_{02} is described by quadratic equation 2, equation 3 can be rewritten as

$$V_{\mathrm{NMO,het}}^{-2} = V_{\mathrm{NMO,hom}}^{-2} - \frac{2\,\tau_0\,\tau_{02}\,D\,k_{x2}^{(2)}}{3V_{02}}, \tag{8}$$

where $k_{x2}^{(2)}$ is the quadratic coefficient for the second layer. Since lateral heterogeneity is assumed to be weak, equation 8 can be linearized in the $k_{x2}^{(2)}$-term:

$$V_{\mathrm{NMO,het}} = V_{\mathrm{NMO,hom}} + \frac{\tau_0\,\tau_{02}\,D\,V^3_{\mathrm{NMO,hom}}\,k^{(2)}_{x2}}{3V_{02}}. \quad (9)$$

As discussed in Takanashi and Tsvankin (2012), equation 9 can be extended to models with an arbitrary number of LH layers. $V_{\mathrm{NMO,het}}$ is responsible for conventional-spread moveout and usually can be estimated from migration velocity analysis (unless there are abrupt lateral velocity changes caused, for example, by salt domes). Near-offset image gathers generated after prestack depth migration become flat when $V_{\mathrm{NMO,het},T} = V_{\mathrm{NMO,het},M}$, where the subscript T refers to the true model and M to the model used for migration. If $k^{(2)}_{x2}$ is positive (e.g., for a low-velocity lens), neglecting its contribution in equation 9 leads to overstated values of $V_{\mathrm{NMO,hom}}$. Likewise, neglecting negative $k^{(2)}_{x2}$ (or a high-velocity lens) leads to understated $V_{\mathrm{NMO,hom}}$.

The k_{x2}-related error in the effective NMO velocity increases with target depth because both τ_0 and D become larger (Takanashi and Tsvankin, 2012). Thus, the moveout in image gathers for deep reflectors is highly sensitive to the error in k_{x2} (i.e., to the difference $k_{x2,M} - k_{x2,T}$) in the overburden. The influence of k_{x2} also distorts the interval NMO velocity (or the parameter δ if the vertical velocity is known) in the deeper part of the section. Note that a constant lateral velocity gradient does not significantly influence the NMO velocity for deeper events, as indicated by the absence of the gradient $k^{(2)}_{x1}$ in equation 8.

Synthetic tests in Takanashi and Tsvankin (2011) also show that velocity lenses in the overburden cause errors in the anellipticity parameter η obtained from nonhyperbolic moveout inversion. According to the analytic results of Grechka (1998), the estimated η depends on second and fourth lateral derivatives of the vertical velocity and, therefore, on k_{x2}.

The influence of errors in k_{x1} and k_{x2} in a thin layer on image gathers obtained after Kirchhoff prestack depth migration is illustrated in Figure 1. For the model in Figure 1, the contribution of either k_{x1} (Figure 2a) or k_{x2} (Figure 2b) leads to a velocity variation of 960 m/s between $x = -2$ km and $x = 2$ km. Prestack synthetic data for all examples in the paper are produced by a finite-difference algorithm (fourth-order in space, second-order in time) using Seismic Unix code "suea2df" (Juhlin, 1995).

Although setting k_{x1} to zero leads to inaccurate V_0 at $x \neq 0$ and distorts positions of the reflectors, the residual moveout in image gathers is small at all depths (Figure 1d). In contrast, ignoring k_{x2} causes a substantial overcorrection (i.e., the imaged depth decreases with offset) for the reflections from interfaces far below the LH layer (Figure 1c). Consequently, failure to account for k_{x2}

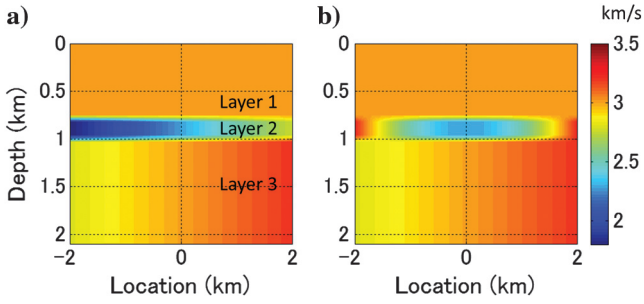

Figure 2. Velocity (V_0) fields used to produce synthetic data for the tests in Figure 1. The parameters of the laterally heterogeneous thin layer are (a) $V_0(x=0) = 2280$ m/s, $k_{x1} = 0.24$ s^{-1}, and $k_{x2} = 0$ and (b) $V_0(x=0) = 2280$ m/s, $k_{x1} = 0$, and $k_{x2} = 2.4 \times 10^{-4}$ s^{-1} m^{-1}. The other parameters are listed in the caption of Figure 1.

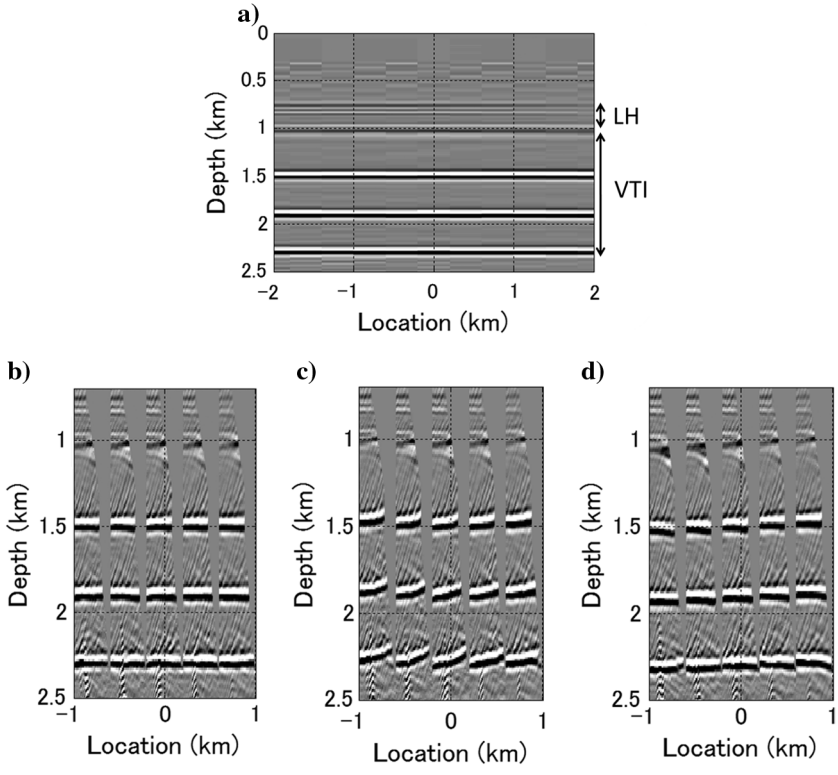

Figure 1. (a) Image of a horizontally layered model obtained by anisotropic prestack depth migration with the actual medium parameters. The top layer is homogeneous and isotropic with $V_0 = 3000$ m/s. The parameters of the laterally heterogeneous (LH) isotropic layer are $V_0(x=0) = 2280$ m/s, $k_{x1} = 0$, and $k_{x2} = 2.4 \times 10^{-4}$ s^{-1} m^{-1} (Figure 2b). The VTI medium beneath the LH layer has $V_0(x=0) = 3000$ m/s, $k_{x1} = 0.1$ s^{-1}, $k_{z1} = 0$, $\varepsilon = 0.2$, and $\delta = 0.1$. The three reflectors embedded in the VTI halfspace represent density contrasts. Image gathers (the maximum offset is 4 km) for the horizontal coordinates ranging between -1 km and 1 km produced (b) with the actual model parameters, and (c) with $k_{x2} = 0$ in the thin LH layer (the other model parameters are correct). (d) Image gathers produced with $k_{x1} = k_{x2} = 0$ in the thin LH layer for a model in which the actual parameters of that layer are $V_0(x=0) = 2280$ m/s, $k_{x1} = 0.24$ s^{-1}, and $k_{x2} = 0$ (Figure 2a).

results in distorted medium parameters at depth. Indeed, it was demonstrated on field data that iterative application of prestack depth migration and velocity updating without correcting for the influence of small-scale lateral heterogeneity amplifies the residual moveout and parameter errors for deep reflectors (e.g., Takanashi et al., 2009).

TTI model with quadratic velocity variation

Next, we analyze image gathers for a layered tilted TI model with quadratic velocity variation. The symmetry axis is taken orthogonal to the bottom reflector in each block, and the symmetry-direction velocity V_0 is represented as

$$V_0(\bar{x},\bar{z}) = V_0(0,0) + \bar{k}_{x1}\,\bar{x} + \bar{k}_{z1}\,\bar{z} + \bar{k}_{x2}\,\bar{x}^2, \qquad (10)$$

where $\bar{x}$ is the distance along the layer boundaries, the $\bar{z}$-axis is perpendicular to them, and $\bar{k}_{x1}$, $\bar{k}_{z1}$, and $\bar{k}_{x2}$ are the parameters in the rotated coordinates (Figure 3). Equation 10 becomes identical to equation 2 if the layer is horizontal. Such TTI model may represent channel-filled or turbidite sands embedded in shaly deposits, which are often found in continental slope areas (Contreras and Latimer, 2010; van Hoek et al., 2010).

As is the case for VTI media, the moveout distortion in image gathers is primarily caused by $\bar{k}_{x2}$, while errors in $\bar{k}_{x1}$ do not produce significant residual moveout (Figure 4). Therefore, the coefficients k_{x2} and $\bar{k}_{x2}$ should play a key role in migration velocity analysis for VTI and TTI models.

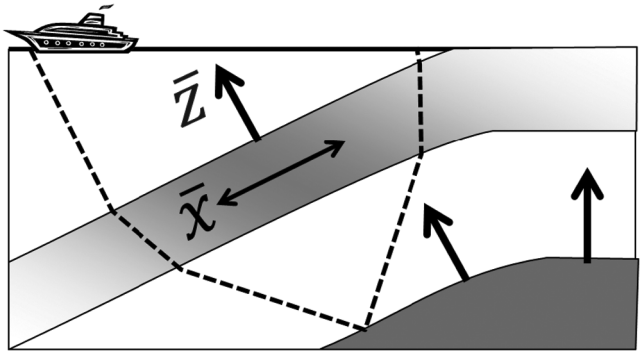

Figure 3. Schematic section of a three-layer TTI model. The symmetry-direction velocity V_0 varies as a quadratic function of the distance along the layer boundaries. The symmetry axis of the TTI layer is perpendicular to its bottom.

Figure 4. (a) Image of a dipping TTI model (maximum dip of 20°) obtained by anisotropic prestack depth migration with the actual medium parameters. The top layer is homogeneous and isotropic with $V_0 = 3000$ m/s. The parameters of the LH layer are $V_0(x = 0, z = 0.75$ km$) = 2280$ m/s, $\bar{k}_{x1} = 0.24$ s^{-1}, and $\bar{k}_{x2} = 2.4 \times 10^{-4}$ s^{-1} m^{-1}. The parameters of the TTI medium beneath the LH layer are $V_0(x = 0, z = 1$ km$) = 3000$ m/s, $\bar{k}_{x1} = 0.1$ s^{-1}, $\bar{k}_{z1} = 0$, $\varepsilon = 0.2$, and $\delta = 0.1$; the symmetry axis is orthogonal to the layer's bottom. Image gathers produced with (b) the actual velocity model, (c) $\bar{k}_{x1} = 0$, and (d) $\bar{k}_{x2} = 0$ in the LH layer (the other parameters are correct). The maximum offset is 4.5 km.

MVA FOR MODELS WITH QUADRATIC VELOCITY VARIATION

As in conventional MVA algorithms, we iteratively apply Kirchhoff PSDM and velocity update until residual moveout becomes sufficiently small. To estimate residual moveout for long-offset data, Sarkar and Tsvankin (2004) introduce the following nonhyperbolic equation in the migrated domain:

$$z_M^2(h) \approx z_M^2(0) + Ah^2 + B\frac{h^4}{h^2 + z_M^2(0)}, \qquad (11)$$

where z_M is the migrated depth, h is the half-offset, and the coefficients A and B are responsible for the residual moveout (the influence of B increases with offset). Equation 11 is employed

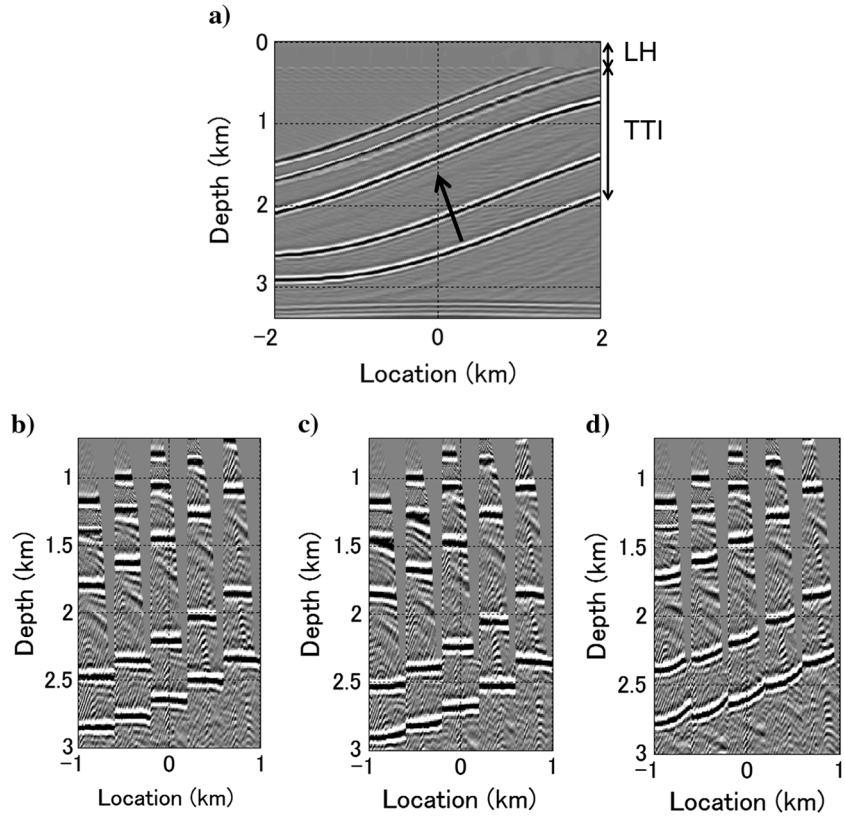

in two-dimensional semblance analysis with the goal of evaluating the magnitude of the residual moveout. In our model, each block is described by the parameters V_0, δ, ε, k_{x1}, k_{z1}, and k_{x2} (or $\bar{k}_{x2}$ for TTI models; the velocity gradient can be described by k_{x1} and k_{z1} instead of $\bar{k}_{x1}$ and $\bar{k}_{z1}$).

Inversion for the parameters of a thin layer in the layer-stripping mode is generally unstable (e.g., Sarkar and Tsvankin, 2004). Also, the moveout for the bottom of the thin layer in Figures 1 and 4 is distorted by NMO stretch, which can lead to further instability in the parameter updates. However, the residual moveout of deep events is quite sensitive to errors in the coefficient k_{x2} in the overburden. Therefore, it is beneficial to minimize the residual moveout for reflectors at all depths simultaneously, particularly when a model includes intervals with quadratic lateral velocity variation. A method for simultaneous estimation of the anellipticity parameter η in multiple layers was introduced by Alkhalifah and Rampton (2001), who examined η as a lithology indicator. The concept of inverting simultaneously for the interval parameters of anisotropic layers also has been used in stacking-velocity tomography (Grechka et al., 2002a, 2002b).

To make the algorithm of Sarkar and Tsvankin (2004) suitable for such simultaneous parameter update, the perturbations of the migrated depths are expressed as linear functions of the perturbations of the medium parameters in all blocks. Then the velocity updates are implemented using the linearized technique of Sarkar and Tsvankin (2004). The migrated depths $z(x_j, h_k)$ (x_j is the midpoint of the jth image gather and h_k is the half-offset) after each iteration are expressed as

$$z(x_j, h_k) = z_0(x_j, h_k) + \sum_{c=1}^{W} \sum_{i=1}^{N} \frac{\partial z_0(x_j, h_k)}{\partial \lambda_{ic}} \Delta\lambda_{ic}, \qquad (12)$$

where W is the number of blocks ($c = 1, 2, \ldots W$), $\partial z_0(x_j, h_k)/\partial\lambda_{ic}$ are the derivatives of the migrated depths with respect to the medium parameters λ_{ic} ($i = 1, 2, \ldots, N$) of block c, and $\Delta\lambda_{ic}$ are the desired parameter updates. To find the updated parameters that minimize the residual moveout for all CMP locations and available reflectors, Sarkar and Tsvankin (2004) apply the least-squares method. The derivatives $\partial z_0(x_j, h_k)/\partial\lambda_{ic}$ are found from anisotropic ray tracing.

SYNTHETIC TESTS

Three-layer VTI model

First, the developed MVA algorithm is tested on a horizontally layered model where quadratic velocity variation is confined to a thin, isotropic middle layer (Figure 5a). The two reflectors located below the LH layer are embedded in a factorized VTI halfspace. Kirchhoff prestack depth migration with the actual model parameters generates an accurate image of all reflectors.

To carry out MVA, we produce image gathers at horizontal coordinates ranging from −2 km to 2 km with a maximum offset of 4 km. The depth profile of the vertical velocity is assumed to be known at one location (here, $x = 0$). For example, V_0 and k_{z1} may be found from check shots or sonic logs acquired in a vertical borehole. The initial model is composed of laterally homogeneous, isotropic layers. The thickness of the LH layer for $x \neq 0$ is updated at each iteration according to the depth of its bottom.

Image gathers obtained with the initial model parameters exhibit substantial residual moveout (Figure 6b). The reflector depths are distorted, and the moveout of the horizontal events in layer 3 is significantly overcorrected. Velocity updating is based on the residual moveout of the two horizontal events in layer 3, which are migrated to incorrect depths (the reflector at the bottom of layer 2 is not used). After five iterations, the residual moveout for all reflectors is practically eliminated, and the reflectors are properly positioned (Figure 6). The estimated coefficients k_{x1} and k_{x2} for layer 2, as well as the parameters of layer 3, are close to the actual values (Figure 7a). These results confirm that the residual moveout of deep reflectors can be used to constrain the coefficient k_{x2} in a thin shallow layer.

For comparison, we process the same synthetic data set using the layer-stripping method of Sarkar and Tsvankin (2004), who employ the linear function $V_0(x, z)$ defined in equation 1. The coefficient k_{x2} is set to zero because the velocity variation in each layer is supposed to be linear. The parameters of the second (LH) layer are estimated using the reflection from the bottom of that layer. The residual moveout after parameter updating (Figure 6d) is only slightly greater than that in Figure 6c. However, the reflector positions are inaccurate and the estimated values of ε and δ in layer 3 are overstated by about 0.05 (Figure 7b). These results indicate that the traveltime error caused by ignoring k_{x2} in layer 2 is largely compensated by distorted parameters in layer 3.

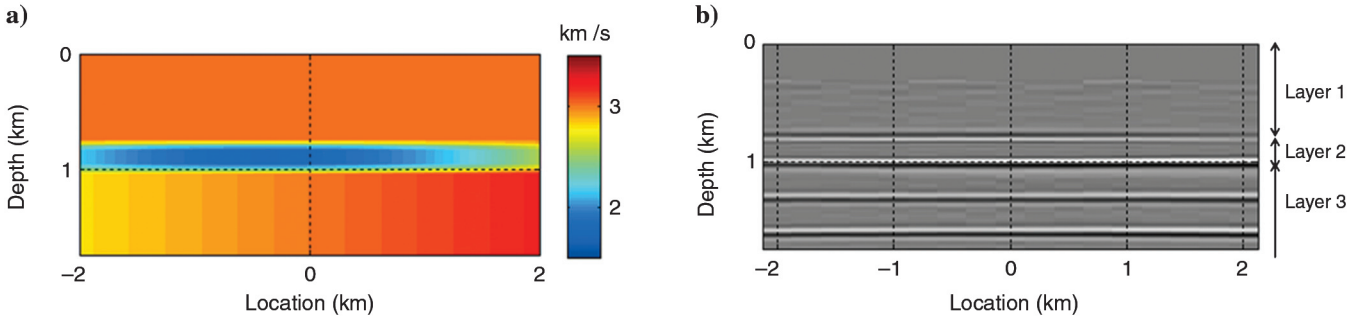

Figure 5. (a) Model composed of three horizontal layers with quadratic lateral velocity variation in the second layer. The top layer (layer 1) is homogeneous and isotropic with $V_0 = 3$ km/s. Layer 2 is isotropic with $V_0 = 1.8$ km/s, $k_{x1} = 0.1$ s^{-1}, and $k_{x2} = 1.3 \times 10^{-4}$ s^{-1} m^{-1}. Layer 3 is factorized VTI with $V_0 = 3$ km/s, $k_{x1} = 0.1$ s^{-1}, $k_{x2} = 0$, $\varepsilon = 0.2$, and $\delta = 0.1$. (b) Image after prestack depth migration with the actual model parameters.

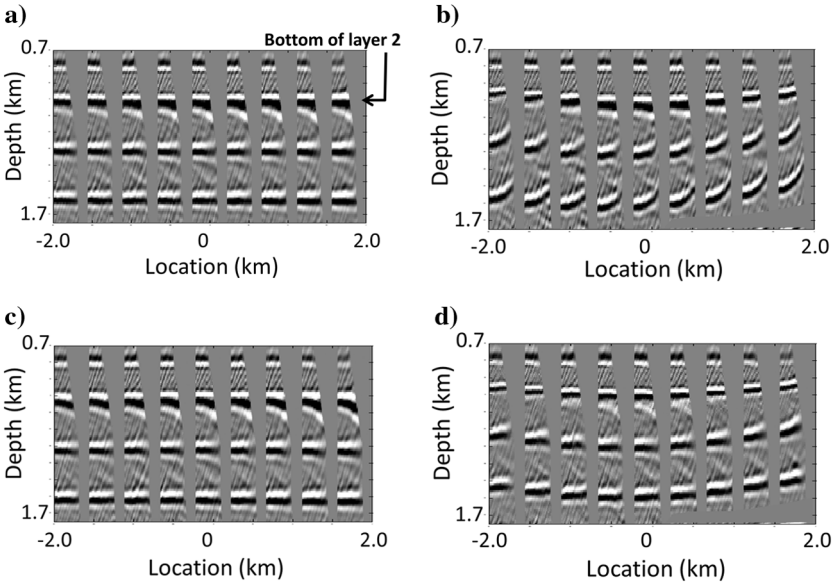

Figure 6. Image gathers for the model in Figure 5 obtained with (a) the actual model parameters; (b) the laterally homogeneous, isotropic initial model; (c) the model estimated by MVA; (d) the parameters estimated in the layer-stripping mode with fixed $k_{x2} = 0$ in layers 2 and 3. The maximum offset is 4 km.

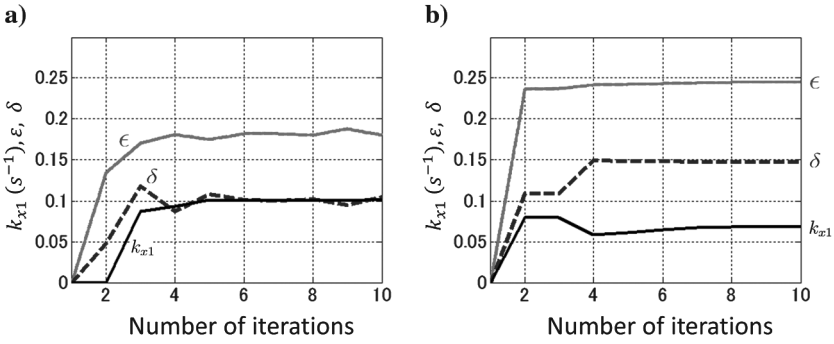

Figure 7. Estimated parameters of layer 3 for the model from Figure 5 using (a) the presented algorithm and (b) MVA applied in the layer-stripping mode. The coefficients k_{x2} estimated by our algorithm are 1.3×10^{-4} s^{-1} m^{-1} in layer 2 and 5.0×10^{-6} s^{-1} m^{-1} in layer 3.

Table 1. Influence of correlated traveltime errors on the estimated parameters of layer 3 for the model in Figure 5. A sinusoidal error function [$t = A \sin(n\pi x/x_{\max})$] was added to each prestack trace.

	Coefficients of error function		
Parameter error	$A = 8$ ms $n = 1$	$A = 8$ ms $n = 2$	$A = 8$ ms $n = 8$
ε	0.05	0.05	0.02
δ	0.05	0.01	0.00
k_{x1} (s^{-1})	0.01	0.00	0.00

Influence of noise

The influence of random noise on MVA results for TI media is evaluated in Sarkar and Tsvankin (2004) and Behera and Tsvankin (2009). They conclude that even relatively strong random noise is mitigated by prestack migration and does not significantly distort parameter estimates. Our testing confirms that uncorrelated traveltime errors have little influence on the output of MVA because they are suppressed by semblance analysis (equation 11).

Migration velocity analysis, however, may be sensitive to correlated traveltime errors (Grechka and Tsvankin, 1998; Takanashi and Tsvankin, 2011). Following Wang and Tsvankin (2009), we assess the influence of correlated errors by contaminating the prestack data for the model in Figure 5 with a sinusoidal time function [$t = A \sin(n\pi x/x_{\max})$, where $x_{\max}$ is the maximum offset]. Such errors are typically caused by inaccurate statics correction or failure to identify lateral heterogeneity on a scale smaller than spreadlength. The inverted parameters are more distorted for small values of n (Table 1), but even for $A = 8$ ms the errors in ε and δ do not exceed 0.05.

Influence of depth and number of reflectors

It is also important to study the dependence of inversion results on the depth and number of available reflectors in the VTI halfspace. The errors somewhat increase with the distance between layer 2 and the shallowest reflector in layer 3 due to the trade-off between the parameters of these layers, but the inversion remains relatively well constrained for all reflector combinations. However, MVA results become less accurate if the vertical gradient k_{z1} in the third layer is unknown. Because the influence of the coefficient k_{x2} gradually increases with depth, there is a trade-off between the values of k_{x2} in layer 2 and k_{z1} in layer 3. Even when three reflectors well separated in depth are available, errors in ε and δ reach 0.03 and 0.05, respectively (Table 2), and the reflectors are shifted vertically.

Multilayered TTI model

Next, the algorithm is applied to a multilayered TTI model (Table 3) with quadratic velocity variation in two thin isotropic layers (marked "LH" in Figure 8). The thin layers are divided into blocks with a width of 3 km (the block boundaries are at $x = \pm 1.5$ km, marked by the dashed line in Figure 8) to properly handle lateral heterogeneity on the scale close to the effective spreadlength (defined as the maximum distance between the incident and reflected rays in the LH layer). Image gathers are produced for locations between −3.2 km and 3.2 km; the maximum offset is 4.5 km. Using the residual moveout for all reflectors, we invert for

the parameters V_0, k_{x1}, and $\bar{k}_{x2}$ in the thin layers ($k_{z1} = 0$ is assumed to be known) and for k_{x1}, $\bar{k}_{x2}$, ε, and δ in the TTI layers. Reflector depths and layer (or block) thicknesses away from the location $x = 0$ are updated at each iteration. Although for TTI media the symmetry-direction velocity V_0 cannot be obtained directly in a vertical borehole (Wang and Tsvankin, 2010), for purposes of this test we use the correct vertical profile of V_0 at location $x = 0$. After 30 iterations, MVA practically removes the residual moveout for all events (Figure 9b) and accurately recovers the parameters of both isotropic (including $\bar{k}_{x2}$) and TTI layers. The inverted coefficients $\bar{k}_{x2}$ in the three TTI layers are nonzero, but their magnitudes are small. The errors in ε, δ, and k_{x1} in the TTI layers are less than 0.03, 0.01, and 0.01 s^{-1}, respectively (Table 3).

Next, we apply the algorithm with the coefficient $\bar{k}_{x2}$ set to zero and the thin layers subdivided into smaller blocks (1.5 km wide). The block boundaries are located at $x = 0$, ± 1.5 km and ± 3 km. Although MVA ignores $\bar{k}_{x2}$, the velocity variations in the thin layers are well resolved and the errors in the TTI parameters are just slightly higher than those in the previous test. Apparently, it is possible to reproduce quadratic lateral velocity variation by employing narrow blocks with constant gradient k_{x1}. In contrast, running MVA in the layer-stripping mode leads to relatively large residual

Table 2. Errors in the estimated parameters of layers 2 and 3 for the model in Figure 5 for different sets of reflectors used in MVA. The results in the right column are obtained without knowledge of the vertical gradient k_{z1} in layer 3.

		Reflector depths (km)			
	Parameters	1.3, 1.6	1.6, 1.9	1.3, 1.9, 2.5	1.3, 1.9, 2.5 (k_{z1} unknown)
Layer 2	k_{x2} ($s^{-1}m^{-1} \times 10^{-5}$)	3.9	5.7	1.1	5.8
Layer 3	ε	0.02	0.02	0.01	0.03
	δ	0.00	0.04	0.00	0.05
	k_{x1} (s^{-1})	0.00	0.01	0.00	0.01
	k_{z1} (s^{-1})	—	—	—	0.15
	k_{x2} ($s^{-1}\,m^{-1} \times 10^{-5}$)	0.5	1.1	0.2	0.2

Table 3. Actual and estimated parameters of the TTI layers for the model in Figure 8. The two thin isotropic layers are divided into blocks 3 km wide for full MVA and 1.5 km wide for the other two tests. The symmetry-direction velocity V_0 at location $x = 0$ is assumed to be known for all depths.

Layer	Parameters	Actual values	Full MVA	MVA without $\bar{k}_{x2}$	MVA in layer-stripping mode
TTI-1	$V_0(0)$ (km/s)	2.6	—	—	—
	ε	0.2	0.23	0.17	0.27
	δ	0.1	0.10	0.11	0.09
	k_{x1} (s^{-1})	0	0.00	0.03	0.03
	$\bar{k}_{x2}$ ($s^{-1}\,m^{-1} \times 10^{-5}$)	0	−1.4	—	—
TTI-2	$V_0(0)$ (km/s)	3.5	—	—	—
	ε	0.2	0.18	0.22	0.10
	δ	0.1	0.11	0.13	0.21
	k_{x1} (s^{-1})	−0.05	−0.055	−0.04	−0.10
	$\bar{k}_{x2}$ ($s^{-1}\,m^{-1} \times 10^{-5}$)	0	0.5	—	—
TTI-3	$V_0(0)$ (km/s)	4.5	—	—	—
	ε	0.1	0.09	0.09	0.15
	δ	0.1	0.11	0.09	0.01
	k_{x1} (s^{-1})	0	0.00	−0.02	0.04
	$\bar{k}_{x2}$ ($s^{-1}\,m^{-1} \times 10^{-5}$)	0	0.7	—	—

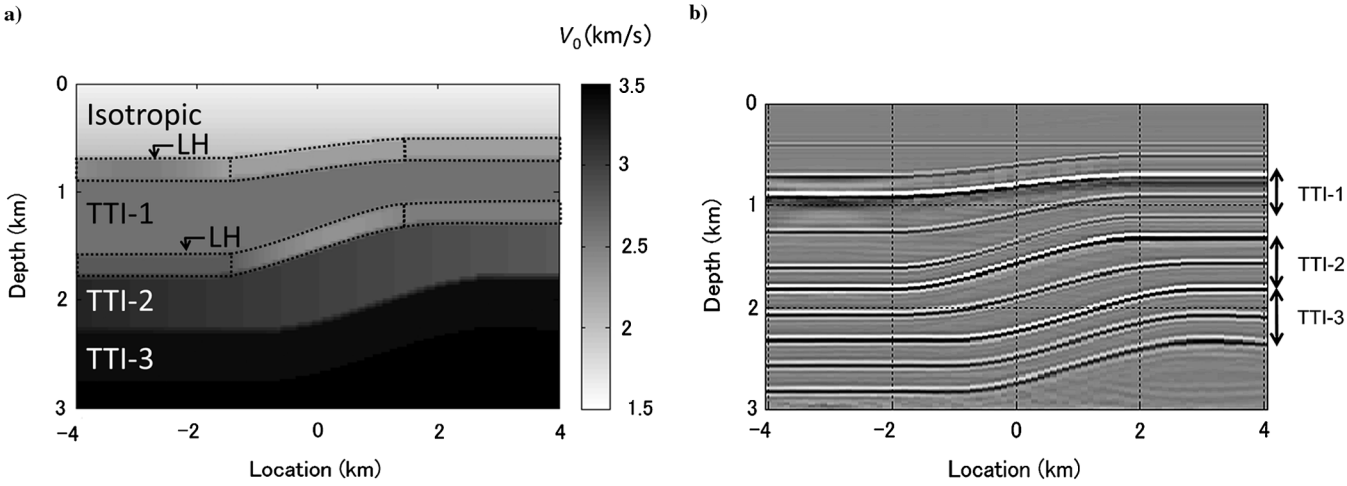

Figure 8. (a) Model that includes three TTI layers. The top layer is isotropic and laterally homogeneous with $V_0(z=0) = 1.6$ km/s and $k_{z1} = 0.5$ s^{-1}. The two thin layers marked "LH" are isotropic and vertically homogeneous with quadratic lateral velocity variation. The parameters of the TTI layers are listed in Table 3. (b) Image after prestack depth migration with the actual model parameters.

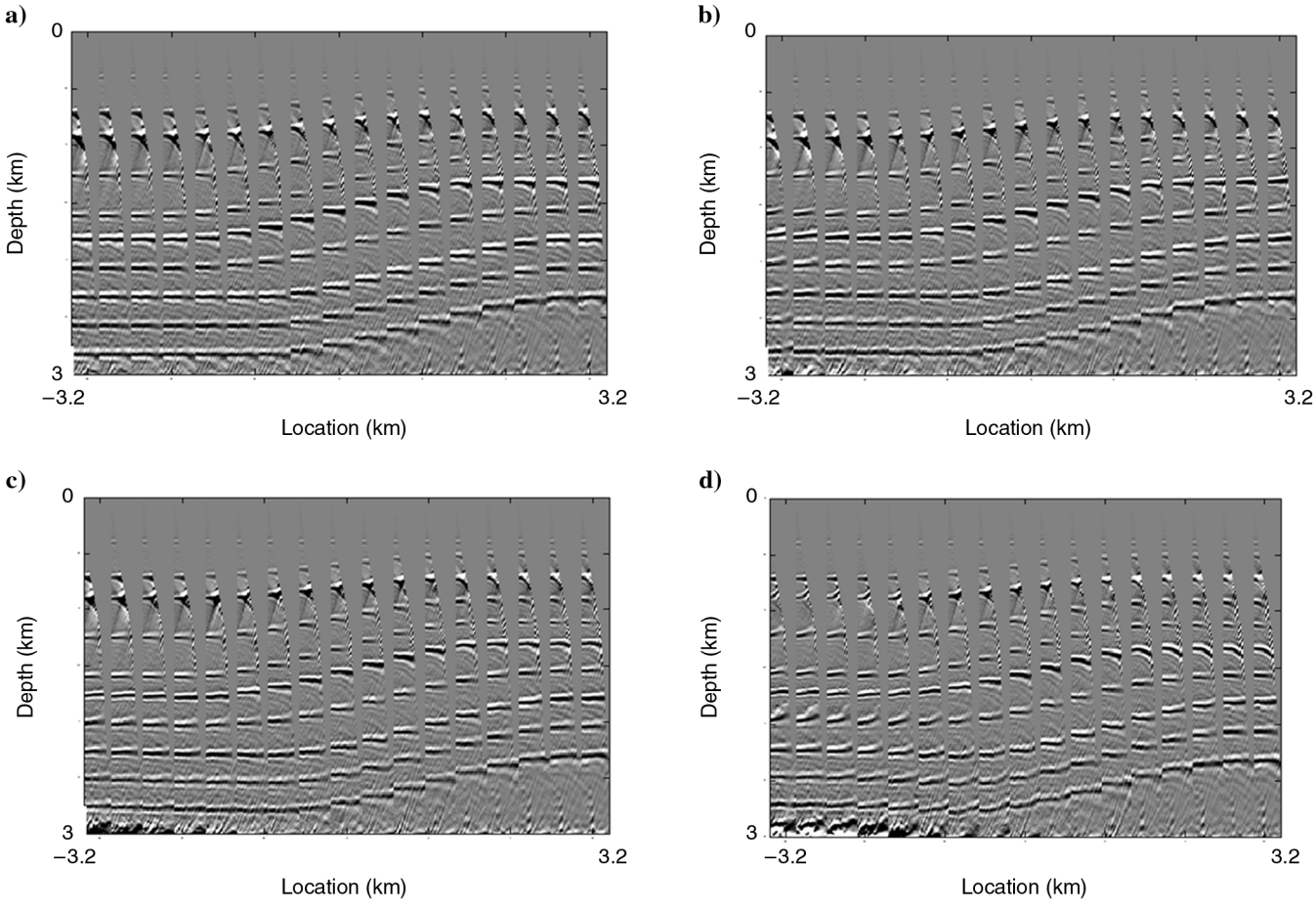

Figure 9. Image gathers for the model from Figure 8 computed using (a) the actual model parameters, (b) the parameters obtained by the presented MVA algorithm ("full MVA"), (c) the parameters obtained by MVA without taking k_{x2} in the thin layers into account (the block width is 1.5 km), and (d) the parameters obtained by MVA in the layer-stripping mode. The estimated parameters of the TTI layers are listed in Table 3. The maximum offset is 4.5 km.

moveout and strongly distorted TTI parameters (Table 3). The instability of parameter estimation in the layer-stripping mode is exacerbated by the NMO stretch at the bottom of the thin LH layers (Figure 9).

CONCLUSIONS

In the first part of the paper, we analyzed the influence of small-scale lateral velocity variation in thin layers on P-wave image gathers for VTI and TTI media (the symmetry axis in TTI layers is taken orthogonal to the reflectors). Analytic and numerical results demonstrate that the quadratic variation of the symmetry-direction velocity V_0 (controlled by the coefficient k_{x2}) strongly influences the residual moveout for deeper reflectors. Even when the vertical profile of V_0 is known, an inaccurate value of k_{x2} can lead to serious distortions in the parameters (such as Thomsen's δ) of the target layer. In contrast, linear lateral velocity variation (i.e., constant lateral velocity gradient) does not produce significant residual moveout at depth.

To account for heterogeneity on a scale smaller than spreadlength, we extended migration velocity analysis to TI media with quadratic lateral velocity variation. The models are composed of factorized VTI and quasi-factorized TTI blocks or layers, in which the parameters ε and δ are constant and the symmetry axis is orthogonal to reflectors. The MVA algorithm simultaneously inverts for the parameters of all layers, which helps constrain the coefficient k_{x2} in the overburden. Because the k_{x2}-induced errors in NMO velocity gradually increase with depth, stable parameter estimation requires information about the vertical gradient k_{z1} if k_{x2} is unknown. Under the assumption that the vertical profile of V_0 is available at one location in each block, the algorithm accurately reconstructs the laterally varying velocity fields and anisotropy parameters throughout the model. Although random traveltime errors are largely suppressed by 2D semblance analysis, the MVA results may be influenced by correlated errors with the spatial period close to spreadlength.

Even in the presence of quadratic lateral velocity variation, the velocity V_0 in thin layers can be constrained by setting k_{x2} to zero and using small blocks with the width close to half the effective spreadlength. If a block boundary is set close to the apex of the quadratic velocity function (e.g., to the center of a velocity lens) and V_0 is assumed to vary linearly within each block, the algorithm can recover the anisotropy parameters beneath the laterally heterogeneous overburden. Therefore, if the spatial velocity variation and anisotropy parameters in the overburden are found with sufficient accuracy, the positions of deeper reflectors are not significantly influenced by block size and velocity parameterization.

It should be emphasized that in our algorithm the most reliable information about lateral velocity variation in shallow layers is provided by reflections from deep interfaces. In contrast, layer stripping produces much less accurate results because the moveout from the bottom of a thin LH layer is weakly sensitive to the layer parameters. Also, evaluation of the residual moveout for reflections from shallow layers is hampered by waveform distortions, such as the NMO stretch.

In practice, anisotropic velocity models for depth imaging are often built by gridded reflection tomography. The main challenge in applying that approach is ambiguity in parameter estimation caused by a large number of independent unknowns. Despite the addition of regularization terms to the objective function, optimizing the smoothing operator remains a difficult problem. As a result, the coefficients ε and δ are often fixed during parameter updates, which may lead to distortions in the velocity model.

Our method to handle small-scale lateral heterogeneity operates with a much smaller number of unknown parameters than gridded tomography. Dividing the medium into a limited number of quasi-factorized blocks mitigates nonuniqueness and ensures a faster convergence of the inversion algorithm. The proposed model representation becomes inadequate for complicated subsurface structures encountered, for example, in subsalt plays and overthrust environments. Still, our methodology is suitable for many areas (e.g., in offshore Northwest Australia and the Middle East) where the overburden is composed of gently dipping TI layers containing small-scale heterogeneities associated with channels or reefs. Also, the insight into the influence of quadratic velocity variation gained here should be helpful in improving the workflow (in particular, by designing optimal smoothing operators or regularization terms) of reflection tomography.

ACKNOWLEDGMENTS

We are grateful to members of the A(nisotropy)-Team of the Center for Wave Phenomena (CWP) at Colorado School of Mines (CSM) for helpful discussions. We also thank John Etgen, Tariq Alkhalifah, Chandan Kumar, Debashish Sarkar, Marta Woodward, and three anonymous referees for their reviews of the manuscript. This work was supported by Japan Oil, Gas and Metals National Corporation (JOGMEC) and the Consortium Project on Seismic Inverse Methods for Complex Structures at CWP.

REFERENCES

Al-Chalabi, M., 1979, Velocity determination from seismic reflection data: Applied Science Publishers.

Alkhalifah, T., and K. Larner, 1994, Migration error in transversely isotropic media: Geophysics, **59**, 1405–1418, doi: 10.1190/1.1443698.

Alkhalifah, T., and D. Rampton, 2001, Seismic anisotropy in Trinidad: A new tool for lithology prediction: The Leading Edge, **20**, 420–424, doi: 10.1190/1.1438964.

Alkhalifah, T., I. Tsvankin, K. Larner, and J. Toldi, 1996, Velocity analysis and imaging in transversely isotropic media: Methodology and a case study: The Leading Edge, **15**, 371–378, doi: 10.1190/1.1437345.

Bakulin, A., Y. Liu, O. Zdraveva, and K. Lyons, 2010a, Anisotropic model building with wells and horizons: Gulf of Mexico case study comparing different approaches: The Leading Edge, **29**, 1450–1460, doi: 10.1190/1.3525359.

Bakulin, A., M. Woodward, D. Nichols, K. Osypov, and O. Zdraveva, 2010b, Building tilted transversely isotropic depth models using localized anisotropic tomography with well information: Geophysics, **75**, no. 4, D27–D36, doi: 10.1190/1.3453416.

Bakulin, A., M. Woodward, D. Nichols, K. Osypov, and O. Zdraveva, 2010c, Localized anisotropic tomography with well information in VTI media: Geophysics, **75**, no. 5, D37–D45, doi: 10.1190/1.3481702.

Behera, L., and I. Tsvankin, 2009, Migration velocity analysis for tilted TI media: Geophysical Prospecting, **57**, 13–26, doi: 10.1111/gpr.2008.57.issue-1.

Biondi, B., 2007, Angle-domain common-image gathers from anisotropic migration: Geophysics, **72**, no. 2, S81–S91, doi: 10.1190/1.2430561.

Blias, E., 2009, Stacking velocities in the presence of overburden velocity anomalies: Geophysical Prospecting, **57**, 323–341, doi: 10.1111/gpr.2009.57.issue-3.

Calvert, A., E. Jenner, R. Jefferson, R. Bloor, N. Adams, R. Ramkhelawan, and C. S. Clair, 2008, Preserving azimuthal velocity information: Experiences with cross-spread noise attenuation and offset vector tile PreSTM: 78th Annual International Meeting, SEG, Expanded Abstracts, 207–211.

Červený, V., 1989, Ray tracing in factorized anisotropic inhomogeneous media: Geophysical Journal International, **99**, 91–100, doi: 10.1111/gji.1989.99.issue-1.

Charles, S., D. R. Mitchell, R. A. Holt, J. Lin, and J. Mathewson, 2008, Data-driven tomographic velocity analysis in tilted transversely isotropic

media: A 3D case history from the Canadian foothills: Geophysics, **73**, no. 5, VE261–VE268, doi: 10.1190/1.2952915.
Contreras, A., and R. Latimer, 2010, Acoustic impedance as a sequence stratigraphic tool in structurally complex deepwater settings: The Leading Edge, **29**, 1072–1082, doi: 10.1190/1.3485768.
Grechka, V., 1998, Transverse isotropy versus lateral heterogeneity in the inversion of P-wave reflection traveltimes: Geophysics, **63**, 204–212, doi: 10.1190/1.1444314.
Grechka, V., A. Pech, and I. Tsvankin, 2002a, Multicomponent stacking-velocity tomography for transversely isotropic media: Geophysics, **67**, 1564–1574, doi: 10.1190/1.1512802.
Grechka, V., A. Pech, and I. Tsvankin, 2002b, P-wave stacking-velocity tomography for VTI media: Geophysical Prospecting, **50**, 151–168, doi: 10.1046/j.1365-2478.2002.00307.x.
Grechka, V., and I. Tsvankin, 1998, Feasibility of nonhyperbolic moveout inversion in transversely isotropic media: Geophysics, **63**, 957–969, doi: 10.1190/1.1444407.
Grechka, V., and I. Tsvankin, 1999, 3-D moveout inversion in azimuthally anisotropic media with lateral velocity variation: Theory and a case study: Geophysics, **64**, 1202–1218, doi: 10.1190/1.1444627.
Huang, T., S. Xu, J. Wang, G. Ionescu, and M. Richardson, 2008, The benefit of TTI tomography for dual azimuth data in Gulf of Mexico: 78th Annual International Meeting, SEG, Expanded Abstracts, 222–226.
Juhlin, C., 1995, Finite-difference elastic wave propagation in 2D heterogeneous transversely isotropic media: Geophysical Prospecting, **43**, 843–858, doi: 10.1111/gpr.1995.43.issue-6.
Neal, S., N. Hill, and Y. Wang, 2009, Anisotropic velocity modeling and prestack Gaussian-beam depth migration with applications in the deepwater Gulf of Mexico: The Leading Edge, **28**, 1110–1119, doi: 10.1190/1.3236381.
Sarkar, D., and I. Tsvankin, 2003, Analysis of image gathers in factorized VTI media: Geophysics, **68**, 2016–2025, doi: 10.1190/1.1635055.
Sarkar, D., and I. Tsvankin, 2004, Migration velocity analysis in factorized VTI media: Geophysics, **69**, 708–718, doi: 10.1190/1.1759457.
Sarkar, D., and I. Tsvankin, 2006, Anisotropic migration velocity analysis: Application to a data set from West Africa: Geophysical Prospecting, **54**, 575–587, doi: 10.1111/j.1365-2478.2006.00556.x.
Takanashi, M., M. Fujimoto, and D. Chagalov, 2009, Overburden heterogeneity effects in migration velocity analysis: A case study in an offshore Australian field: 71st Annual International Meeting, EAGE, Extended Abstracts.
Takanashi, M., and I. Tsvankin, 2011, Correction for the influence of velocity lenses on nonhyperbolic moveout inversion for VTI media: Geophysics, **76**, no. 3, WA13–WA21, doi: 10.1190/1.3569799.
Takanashi, M., and I. Tsvankin, 2012, Moveout analysis of wide-azimuth data in the presence of lateral velocity variation: Geophysics, **77**, no. 3, U49–U62, doi: 10.1190/geo2011-0307.1.
Toldi, J., 1989, Velocity analysis without picking: Geophysics, **54**, 191–199, doi: 10.1190/1.1442643.
Tsvankin, I., J. Gaiser, V. Grechka, M. van der Baan, and L. Thomsen, 2010, Seismic anisotropy in exploration and reservoir characterization: An overview: Geophysics, **75**, no. 5, 75A15–75A29, doi: 10.1190/1.3481775.
van Hoek, T., S. Gesbert, and J. Pickens, 2010, Geometric attributes for seismic stratigraphic interpretation: The Leading Edge, **29**, 1056–1065, doi: 10.1190/1.3485766.
Wang, X., and I. Tsvankin, 2009, Estimation of interval anisotropy parameters using velocity-independent layer stripping: Geophysics, **74**, no. 5, WB117–WB127, doi: 10.1190/1.3157462.
Wang, X., and I. Tsvankin, 2010, Stacking-velocity inversion with borehole constraints for tilted TI media: Geophysics, **75**, no. 5, D69–D77, doi: 10.1190/1.3481652.
Woodward, M., D. Nichols, O. Zdraveva, P. Whitfield, and T. Johns, 2008, A decade of tomography: Geophysics, **73**, no. 5, VE5–VE11, doi: 10.1190/1.2969907.